ACS Photonics

Letter

Cite This: ACS Photonics XXXX, XXX, XXX−XXX

pubs.acs.org/journal/apchd5

Electrochemistry on Inverse Copper Nanoantennas: Active Plasmonic Devices with Extraordinarily Large Resonance Shift

Annette Böhme,* Florian Sterl, Elinor Kath, Monika Ubl, Venla Manninen, and Harald Giessen

4th Physics Institute and Research Center SCoPE, University of Stuttgart, Pfaffenwaldring 57, 70569 Stuttgart, Germany

Supporting Information

ABSTRACT: Arrays of metallic nanoparticles can be used for plasmonic color printing. However, the development of dynamic plasmonic color displays capable of controllable and reversible switching of individual pixels is still in its infancy. Here, an active plasmonic device that operates at the border between the visible and the near-infrared spectral region using inverse copper nanoantennas is introduced. This is a suitable choice, as copper can easily and reversibly be oxidized and reduced with the method of cyclic voltammetry. The inverse sample setup allows for the easy application of an electrical contact. With this configuration, a centroid wavelength shift of up to 210 nm ($\Delta\lambda/\lambda \approx 25\%$) within less than 3 min can be achieved, which is extraordinarily large. The resonance shift can be reversed, and the response increases with every voltage cycle, which is attributed to structural changes on the copper surface, leading to an increased surface area.

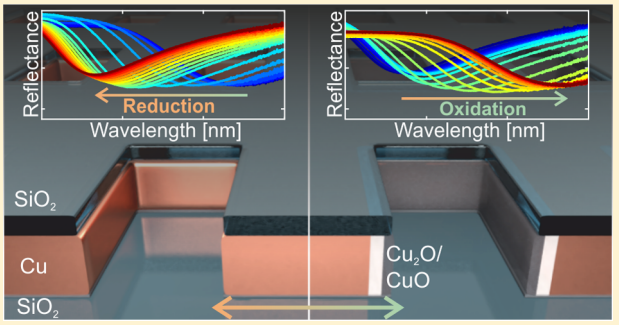

KEYWORDS: *active plasmonics, copper, copper oxide, cyclic voltammetry, Babinet's principle, spectroscopy*

In recent years, a lot of research has been conducted to develop a device whose plasmonic resonance can be externally controlled.[1−8] In fact, the field of active plasmonics offers various fascinating applications, including tunable nano-optics, smart windows, modulators, switches, and dynamic plasmonic color displays with unprecedented resolution and tunability.[9−14] The latter application exploits the principle of plasmonic color printing,[15−17] meaning that bright and nonfading images can be created by patterning arrays of metallic nanoantennas to build plasmonic pixels. In order to not only create static pictures, but dynamic displays, it is not only necessary to create dynamic pixels, but also to be able to address single pixels that can be switched individually. For this, an electrical switching method is ideal, as it allows for an easy control of the setup and enables to contact single pixels.

Several configurations for an active plasmonic device have been proposed already. However, the so far introduced setups are restricted by a limited resonance shift and do not offer the possibility to address individual pixels. As a first step on the road toward individually addressable pixels, the approach in this work is to lithographically manufacture nanoparticles whose dielectric function can be controlled by applying a voltage. The lithographic fabrication allows for the integration of small pixels, consisting of several nanoslits each, into other circuitry, while the electrical switching method allows to implement a design where single pixels can be addressed individually.

The material copper is a very promising choice for this, as it is not only comparably cheap, but also possesses very good plasmonic properties[18,19] and can easily be oxidized and reduced in an electrolyte solution with the method of cyclic voltammetry.[20−24] An inverse sample setup with slits etched into a copper film is possible due to Babinet's principle[25,26] and allows for the easy application of an electrical contact to the sample. This switching principle, using inverse copper nanostructures, is illustrated in Figure 1a,b. The copper inside the slits, facing the electrolyte, is oxidized and reduced in turns, thereby covering and uncovering the metallic copper with the dielectric copper oxides Cu_2O/CuO, which changes the plasmonic properties of the sample.[27] This is confirmed by scattering-matrix simulations using the S-matrix method of T. Weiss,[28] see Figure 1c, illustrating the spectrum of a nanostructured copper sample covered with copper oxides with different thicknesses. A simplified two-layered oxide structure with an inner shell of Cu_2O and an outer shell of CuO is assumed. The oxide layer thickness of 3.3 nm corresponds to 2 nm Cu_2O and 1.3 nm CuO, which roughly is the oxide thickness obtained by air exposure.[29] The other values are multiples of these values, as thicker oxide layers can be obtained by electrochemical means. The dielectric functions of Cu_2O and CuO are quite similar,[30] giving a refractive index at 800 nm of $n = 2.7$ and 2.94, respectively. Upon oxidation, the plasmonic resonance position undergoes a redshift as the refractive indices of Cu_2O and CuO are higher than that of the surrounding electrolyte solution, and additionally, as the Cu facing the nanoslits transforms into the dielectric copper oxides, the metal slits effectively increase in size. Upon the

Received: May 17, 2019
Published: July 19, 2019

DOI: 10.1021/acsphotonics.9b00716
ACS Photonics XXXX, XXX, XXX−XXX

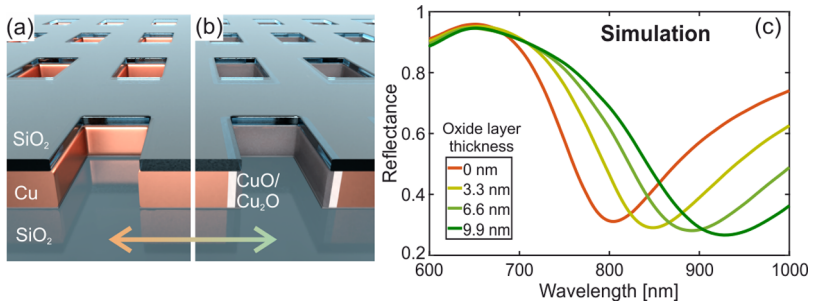

Figure 1. Schematic of the electrochemical switching method applied in this work. The position of the plasmonic resonance is shifted by periodically switching the copper inside the walls of the nanoslits between its elementary and oxidized state with the method of cyclic voltammetry. The metallic copper (a) is thereby in turn covered by the dielectric copper oxides (b), leading to different plasmonic properties. (c) S-matrix simulation of the effect of a copper oxide layer inside copper nanoslits on the spectral response normalized to the reflectance spectrum of an unstructured copper film. For the simulation, a layered structure with 2 nm chromium, 30 nm copper, and 15 nm SiO_2 patterned with slits with a length of 140 nm, a width of 60 nm, and a periodicity in the *x*- and *y*-direction of 300 nm was taken into account. Note that, in reality, the copper directly underneath the SiO_2 layer is also covered with a thin oxide layer caused by air exposure between the two evaporation processes. However, it does not contribute to the switching characteristics of the sample and is, thus, for simplicity not shown.

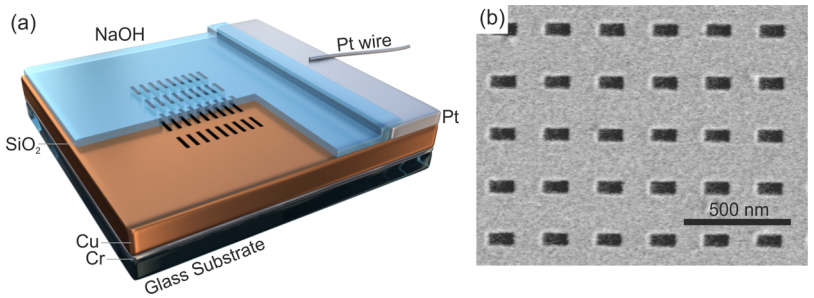

Figure 2. (a) Schematic of the structure of an inverse nanostructured copper sample on a glass substrate with a 2 nm chromium adhesion layer, a 30 nm thick copper film, and a 15 nm protective SiO_2 layer, here cut out for better visibility of the copper film. A 40 nm thick platinum edge for electrical contact, as illustrated by the platinum wire, is depicted as well. In the center of the sample, an array of nanoslits penetrating all three layers with a size of typically 100 μm × 100 μm is visible. During electrochemical experiments, this sample acts as a working electrode and is immersed in an electrolyte solution of 0.1 M NaOH together with a platinum counter electrode and a Hg/HgO reference electrode. (b) SEM image of a nanostructured copper film patterned with the manufacturing method described above, including a protective silicon dioxide layer. The slits show a good rectangular shape and the copper surface is very smooth.

reverse reduction, a corresponding blueshift is anticipated to take place. This gives rise to the expectation that inverse copper nanostructures can indeed be applied for an active plasmonic device with resonances in the visible/near-infrared and could be used for the development of ultrahigh resolution dynamic plasmonic color displays.

METHODS

In order to fabricate samples that meet the requirements for an active plasmonic device with a switching method, as introduced above, we use a sample geometry, as displayed in Figure 2a. A chromium adhesion layer and a platinum edge for electrical contact, as well as a protective SiO_2 layer above the copper film, are introduced. Arrays of nanoslits with a large area and outstanding quality featuring very well pronounced plasmonic resonances are patterned into the film with electron beam lithography and subsequent argon ion beam etching.

On a thoroughly cleaned 10 mm × 10 mm glass substrate, a 2 nm Cr adhesion layer and a 30 nm Cu film are evaporated with thermal evaporation using a Pfeiffer Classic 250 device. For electrical contact during the measurement, a 40 nm Pt edge on an approximately 2 mm wide stripe at the border of the sample is deposited with electron beam evaporation utilizing a Pfeiffer PLS 500 S. On top of the copper surface, a 15 nm SiO_2 layer is evaporated with the same device. This step is essential, as it protects the corrodible copper during aggressive fabrication steps such as heating, physical and chemical etching, and exposure to solvents. Furthermore, the SiO_2 layer ensures that the copper oxidation and reduction process is concentrated inside the nanoslits where it can contribute to the plasmonic resonance shift. As a next step, the high resolution resist AR-P6200.04 is applied to the sample surface with a RAMGRABER PLM 7xx spin-coater and baked at 150 °C for 60 s. The resist is patterned using the method of electron beam lithography with a RAITH Nanofabrication eLINE Plus device with an aperture of 7.5 μm and a dose factor of 1.5. Arrays of a size of 100 μm × 100 μm consisting of rectangular nanoslits with a width of 60 nm, a length of 140 nm, and periodicity in the *x*- and *y*-direction of 300 nm are created. This corresponds to a total of about 100000 slits contributing to the current signal, while only a several μm wide stripe of the full array is considered in the reflectance measurements. For comparison, samples with altering parameters are fabricated as well. After developing the resist, the thereby created patterning mask can be used to etch slits into the SiO_2 protective layer and the copper with argon ion beam etching using a R.I.B. Etching 160 Reactive Ion Beam system. To remove the resist afterward, the sample is placed in the solvent *N*-methyl-2-pyrrolidone (NMP) in an ultrasonic bath heated to 80 °C for several hours. In a last step,

DOI: 10.1021/acsphotonics.9b00716
ACS Photonics XXXX, XXX, XXX−XXX

resputtered edges that form during argon ion beam etching have to be removed with a parallel argon ion beam etching step. The manufacturing process is visualized in Figure S1. The quality of each sample is screened with a HITACHI S-4800 scanning electron microscope (SEM).

With the described manufacturing procedure including a protective SiO_2 layer, high quality nanostructured copper samples featuring well-defined plasmonic resonances can be fabricated. The resulting sample setup is visualized in Figure 2a, while Figure 2b displays an SEM picture of the sample, documenting the high quality of the structures. A both theoretical and experimental study of how the slit size can influence the position and modulation of plasmonic resonances is presented in Figure S2.

To switch the copper inside nanoslits with cyclic voltammetry, the sample is placed in a custom-made electrochemical cell with a three-electrode setup, filled with the alkaline electrolyte solution of 0.1 M NaOH. The copper sample itself acts as the working electrode and is contacted at the Pt edge with a Pt wire, see Figure 2a. The counter electrode is a platinum wire and as a reference electrode, an ALS RE-61AP Hg/HgO reference electrode for alkaline solution is used. The three electrodes are connected to a BioLogic SP-200 potentiostat. Cyclic voltammetry is performed at a scan rate of 5 mV/s between +0.5 V and −1 V vs Hg/HgO for several cycles. For comparison, additional measurements are performed at various scan rates between 2 mV/s and 30 mV/s and with a voltage window between +0.5 V and −0.85 V. During the downscan of the voltage, a two-step reduction process of copper is initiated with the electrochemical reactions $2\ CuO + H_2O + 2\ e^- \rightarrow Cu_2O + 2OH^-$ and $Cu_2O + 2\ e^- + H_2O \rightarrow 2\ Cu + 2OH^-$, while the reverse oxidation process takes place during the upscan.[20−22] The corresponding cyclic voltammogram is displayed in Figure 3.

While performing cyclic voltammetry, the electrochemical cell is mounted onto the stage of a Nikon Eclipse LV100 microscope with a Nikon TU Plan ELWD 20×/0.40 objective.

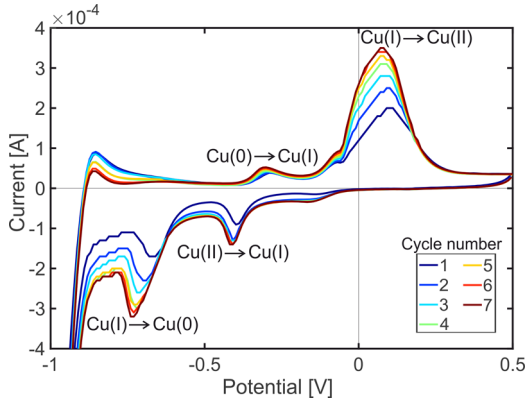

Figure 3. Cyclic voltammogram obtained with a nanostructured copper film at a scan rate of 5 mV/s and a voltage window between +0.5 V and −1 V vs Hg/HgO during seven cycles. One precycle that was performed prior to these measurements is not shown. During the downscan of the voltage, a two-step reduction takes place, including the chemical reactions $2\ CuO + H_2O + 2\ e^- \rightarrow Cu_2O + 2\ OH^-$ (abbreviated with Cu(II) → Cu(I)) and $Cu_2O + 2\ e^- + H_2O \rightarrow 2\ Cu + 2\ OH^-$ (Cu(I) → Cu(0)), while during the upscan, the reverse oxidation processes $Cu_2O + 2\ OH^- \rightarrow 2\ CuO + H_2O + 2\ e^-$ (Cu(0) → Cu(I)) and $2\ Cu + 2\ OH^- \rightarrow Cu_2O + 2\ e^- + H_2O$ (Cu(I) → Cu(II)) take place.

The spectral response of the sample is tracked through a glass window in the electrochemical cell. The sample is illuminated with an Energetiq LDLS EQ-99 laser driven light source with the incident light polarized along the short axis of the nanoslits. Optical images are recorded with an Allied Vision GC2450c camera. Visible and near-infrared reflectance spectra are tracked with a Princeton Instruments Isoplane 160 spectrometer with a Princeton Instruments PIXIS-256 CCD camera. A smooth copper surface is used as reference position for spectral measurements. The entire setup is available at NT&C.[31]

RESULTS AND DISCUSSION

This switching principle introduced in Figure 1 could successfully be implemented experimentally. Figure 4 displays the spectral response of a copper film nanostructured as explained above upon electrochemical switching during the fifth cycle of cyclic voltammetry. A distinct resonance shift in the order of 200 nm within approximately 2.5 min is visible. Figure S3 displays additional spectral data for all first six cycles.

The full spectral behavior over the entire course of the measurement is visible in the color map of Figure 5a, displaying absolute wavelength- and time-resolved reflectance data encoded in color. The resonance position shifts with the same periodicity as the voltage. After the sixth cycle, the resonance position starts to shift out of the measurable range above wavelengths of 1000 nm. The centroid wavelength position[32] is extracted for all times before this is the case (within the black frame in Figure 5a) and is displayed in Figure 5b (blue) together with the cycled voltage (orange). Apart from a distinct, periodic, and repeatable resonance shift following the voltage, we find that the response becomes stronger with every voltage cycle. The increasing signal is attributed to structural changes on the copper surface upon repeated oxidation and reduction. As elementary copper is oxidized electrochemically, Cu_2O nanograins and CuO nanocrystals grow on the copper surface.[33] Even upon subsequent reduction, small copper nanoparticles remain on the surface, increasing the surface area of the active copper inside the nanoslits. SEM images of a nanostructured copper surface confirm this (see Figure S4a). Hence, the working surface is enhanced, leading to more oxide growth with every voltage cycle and, therefore, an increasing shifting response with a self-enhancing effect.

In addition to an increasing signal, an overall redshift of the centroid wavelength position can be observed in Figure 5b. This behavior is explained by considering that the copper sample slowly dissolves during electrochemical measurements as CuO undergoes a chemical reaction with the electrolyte NaOH,[34] leading to the slow dissolution of the copper film; compare Figure S3a. As the copper is covered with a protective SiO_2 layer, the dissolution does not happen uniformly over the entire copper film, but starts where the SiO_2 is thinnest, leading to a porous film with small electrolyte-filled cavities. The increasing porosity, together with an overall decreasing film thickness, leads to a distinct red shift of the plasmonic resonance. This is confirmed by an effective medium simulation using the Bruggeman model[35,36] and S-matrix simulations,[28] showing that, for an increasing ratio of water-filled cavities enclosed in the copper film, the plasmonic resonance position undergoes a distinct red shift, see Figure S4b. This effect causes a slow red shift of the resonance, even upon applying a constant potential; however, a stable signal

DOI: 10.1021/acsphotonics.9b00716
ACS Photonics XXXX, XXX, XXX−XXX

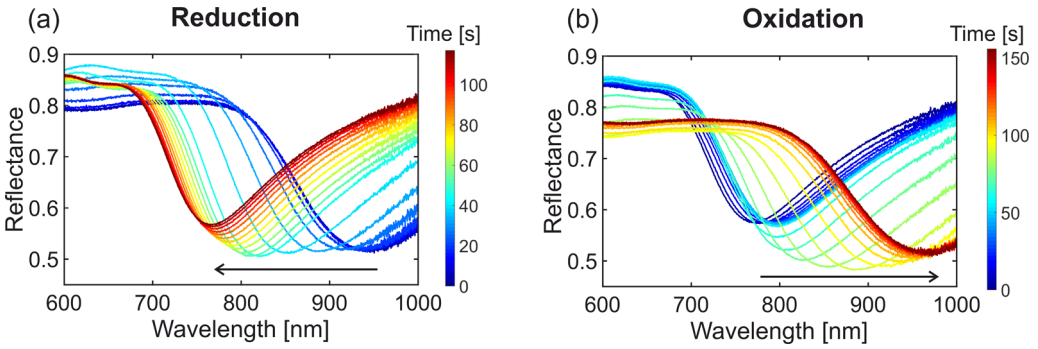

Figure 4. Spectral shift of the plasmonic resonance of an inverse copper nanostructure with a film thickness of 30 nm, a length of the slits of 140 nm, width of the slits of 60 nm, and a periodicity in the *x*- and *y*-direction of 300 nm during (a) reduction and (b) oxidation with cyclic voltammetry during the fifth voltage cycle. Measurements were performed with a scan rate of 5 mV/s between +0.5 V and −1.0 V vs Hg/HgO, linear polarization is along the short axis of the nanoslits, exciting the fundamental LSPR resonance. The resonance position undergoes a blue shift of as much as 180 nm during reduction and a red shift of 203 nm during oxidation. For spectra obtained during other cycles, see Figure S2.

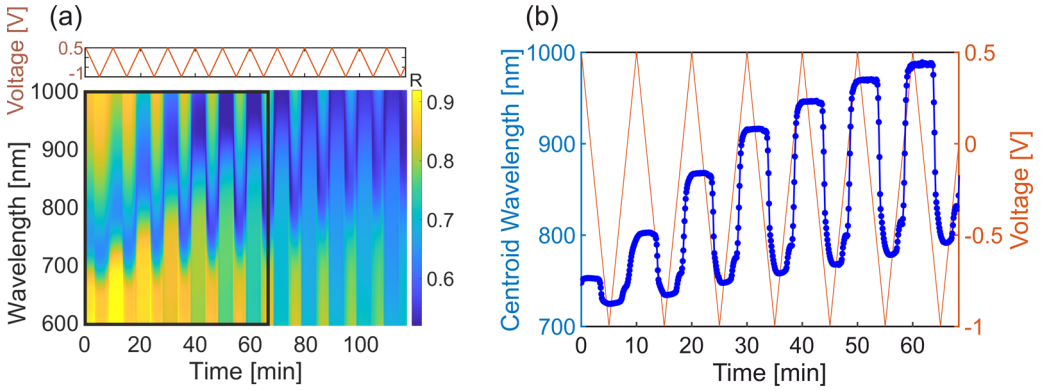

Figure 5. (a) Cycling voltage (top) and color map of reflectance encoded in the color bar over time (bottom) during cyclic voltammetry with a scan rate of 5 mV/s. The map displays the full spectral behavior, particularly the shift of the absolute reflectance value. The time interval within the black frame is further investigated in (b), displaying the centroid wavelength of the plasmonic resonance spectrum during cyclic voltammetry (blue) together with the periodically sweeped voltage (orange). At times exceeding the displayed interval, the centroid wavelength begins to shift out of the measurable wavelength range above 1000 nm. The plasmonic resonance shifts considerably with the same periodicity as the voltage by up to 210 nm within 2.5 min. With every voltage cycle, the response becomes stronger and the plasmonic resonance undergoes an overall redshift.

could be obtained if a method was developed that prevents the slow dissolution of the copper film.

Considering once more Figure 5a, the vertical stripes indicate that not only the plasmonic resonance position undergoes a shift, but also the absolute reflectance intensity is subject to a periodic shift. The shift of the reflectance intensity at the centroid wavelength position is extracted in Figure S5. Upon reduction, the intensity is increased while it decreases during oxidation, which can be explained by considering that smooth copper has a higher reflectance compared to the darker and rougher copper oxides. For scan rates of 5 mV/s and less, however, a reversed plateau is observable for the fully oxidized state, indicating the full overgrowing of nanoslits with oxides. This implies that oxide growing and the connected plasmonic response is stronger for low scan rates. Overall, the reflectance intensity decreases, which is again caused by the slow dissolution of the copper film, as explained above, leading to a thinner and rougher film with more light transmission and scattering and, hence, a lower reflectance.

In order to investigate the influence of different sample and measurement parameters on the switching behavior, several measurements with altering parameters were performed. It makes sense that with a faster scan rate the switching is quicker as the time needed for one switching cycle corresponds to that of one voltage cycle. However, the switching response is considerably higher upon slow cycling, as already indicated by the fact that slow scan rates correspond to a stronger oxide growth. Consider Figure S6, showing the centroid wavelength shift over time for a measurement performed at a scan rate of 20 mV/s as compared to 5 mV/s, as displayed in Figure 5b. During the fifth oxidation process, a centroid wavelength shift of 203 nm is achieved for the scan rate of 5 mV/s, while for the higher rate of 20 mV/s, it is only 81 nm. This indicates again that saturation of the resonance shift is only achieved for low scan rates of 5 mV/s and less.

The sample stability is not influenced by the scan rate (compare Figure S7a), nor by the voltage window used (Figure S7b) or the thickness of the SiO_2 layer (Figure S7c). However, the stability during electrochemical measurements can be improved by using a thinner copper film (Figure S7d), which can be explained by considering that, for thicker films, the argon ion beam etching step during sample preparation has to be longer, therefore, attacking the patterning mask resist and, if exceeding a certain amount of time, the sample itself. Therefore, the sample quality is improved for thinner films. In addition, the sample stability is clearly improved by reducing the width of the nanoslits (Figure S7e), easily explicable by taking into account that, for narrow slits, the surface area of copper exposed to the electrolyte and the amount of electrolyte that can penetrate into the slits is limited.

DOI: 10.1021/acsphotonics.9b00716
ACS Photonics XXXX, XXX, XXX−XXX

CONCLUSION AND OUTLOOK

An active plasmonic device with a resonance shift of 210 nm in the visible to near-infrared range within 2.5 min was successfully implemented with the use of inverse copper nanoantennas. The obtained shift is among the highest reported in literature so far.[37] Switching can be performed electrochemically with the method of cyclic voltammetry to switch copper inside nanoslits between the elementary and the oxidized state. The response upon switching increases with every voltage cycle due to structural changes on the copper surface. The response is slower but significantly enhanced for slow scan rates around 5 mV/s. The sample stability can be improved by using thin copper films with narrow slits. It could be further enhanced by performing experiments with a different electrolyte solution. Future steps toward the development of pixelated active plasmonic devices include to downscale the experiments to smaller arrays or even single slits that can be addressed individually and to use oxygen donors incorporated in a solid instead of the aqueous NaOH electrolyte solution to develop an all-solid device with increased stability. Additionally, different plasmonic geometries such as perfect absorbers[38,39] as well as Fano resonant structures[40] could be used to improve modulation depth and wavelength selectivity. To enhance the accessible wavelength range especially in the visible spectral range, it could be useful to introduce other oxidizable materials than copper. Our sample geometry might also be utilized for the resonant vibrational detection of carbon monoxide molecules as a product of the electrochemical reduction of carbon dioxide with copper as a catalyst as the plasmon resonance can be tuned to 2080 cm^{-1} (see Figure S8).

ASSOCIATED CONTENT

Supporting Information

The Supporting Information is available free of charge on the ACS Publications website at DOI: 10.1021/acsphotonics.9b00716.

> Overview of manufacturing process. Spectral data for six successive reduction and oxidation cycles. Explanation for increasing response and an overall redshift of the centroid wavelength. Reflectance at centroid wavelength. Centroid wavelength for scan rate 20 mV/s. Relation between sample stability and sample and measuring parameters. Sample configuration as usable for the sensing of CO molecules (PDF)

AUTHOR INFORMATION

Corresponding Author

*E-mail: annetteboehme@gmail.com.

ORCID

Annette Böhme: 0000-0003-1109-3428

Florian Sterl: 0000-0002-1025-6777

Author Contributions

The manuscript was written through contributions of all authors. All authors have given approval to the final version of the manuscript.

Notes

The authors declare no competing financial interest.

ACKNOWLEDGMENTS

We gratefully acknowledge financial support by the Deutsche Forschungsgemeinschaft (SPP1391 and 1839), by the Bundesministerium für Bildung und Forschung, by ERC Advanced Grant COMPLEXPLAS, by the Baden-Württemberg Stiftung, and by the Ministerium für Wissenschaft, Forschung und Kunst Baden-Württemberg. We would furthermore like to thank Mario Hentschel and Bettina Frank for discussions and valuable help.

REFERENCES

(1) Grinblat, G.; Berté, R.; Nielsen, M. P.; Li, Y.; Oulton, R. F.; Maier, S. A. Sub-20 Fs All-Optical Switching in a Single Au-Clad Si Nanodisk. *Nano Lett.* **2018**, *18*, 7896−7900.

(2) Leroux, Y.; Lacroix, J. C.; Fave, C.; Trippe, G.; Felidj, N.; Aubard, J.; Hohenau, A.; Krenn, J. R. Tunable Electrochemical Switch of the Nanoparticles. *ACS Nano* **2008**, *2*, 728−732.

(3) Stockhausen, V.; Martin, P.; Ghilane, J.; Leroux, Y.; Randriamahazaka, H.; Grand, J.; Felidj, N.; Lacroix, J. C. Giant Plasmon Resonance Shift Using Poly(3,4-Ethylenedioxythiophene) Electrochemical Switching. *J. Am. Chem. Soc.* **2010**, *132*, 10224−10226.

(4) Sterl, F.; Strohfeldt, N.; Walter, R.; Griessen, R.; Tittl, A.; Giessen, H. Magnesium as Novel Material for Active Plasmonics in the Visible Wavelength Range. *Nano Lett.* **2015**, *15*, 7949−7955.

(5) Aydin, K.; Burgos, S.; Pryce, I. M.; Dicken, M. J.; Dionne, J. A.; Diest, K.; De Waele, R.; Polman, A.; Atwater, H. A. Active Plasmonic Devices and Optical Metamaterials. *Conf. Proc. - Lasers Electro-Optics Soc. Annu. Meet.* **2009**, *1*, 92−93.

(6) Byers, C. P.; Zhang, H.; Swearer, D. F.; Yorulmaz, M.; Hoener, B. S.; Huang, D.; Hoggard, A.; Chang, W.-S.; Mulvaney, P.; Ringe, E.; et al. From Tunable Core-Shell Nanoparticles to Plasmonic Drawbridges: Active Control of Nanoparticle Optical Properties. *Sci. Adv.* **2015**, *1*, No. e1500988.

(7) Michel, A. K. U.; Zalden, P.; Chigrin, D. N.; Wuttig, M.; Lindenberg, A. M.; Taubner, T. Reversible Optical Switching of Infrared Antenna Resonances with Ultrathin Phase-Change Layers Using Femtosecond Laser Pulses. *ACS Photonics* **2014**, *1*, 833−839.

(8) Dicken, M. J.; Aydin, K.; Pryce, I. M.; Sweatlock, L. A.; Boyd, E. M.; Walavalkar, S.; Ma, J.; Atwater, H. A. Frequency Tunable Near-Infrared Metamaterials Based on VO2 Phase Transition. *Opt. Express* **2009**, *17*, 18330−18339.

(9) Duan, X.; Kamin, S.; Liu, N. Dynamic Plasmonic Colour Display. *Nat. Commun.* **2017**, *8*, 14606.

(10) Chen, Y.; Duan, X.; Matuschek, M.; Zhou, Y.; Neubrech, F.; Duan, H.; Liu, N. Dynamic Color Displays Using Stepwise Cavity Resonators. *Nano Lett.* **2017**, *17*, 5555−5560.

(11) Hoener, B. S.; Kirchner, S. R.; Heiderscheit, T. S.; Collins, S. S. E.; Chang, W. S.; Link, S.; Landes, C. F. Plasmonic Sensing and Control of Single-Nanoparticle Electrochemistry. *Chem.* **2018**, *4*, 1560−1585.

(12) Leroux, Y.; Lacroix, J. C.; Fave, C.; Stockhausen, V.; Felidj, N.; Grand, J.; Hohenau, A.; Krenn, J. R. Active Plasmonic Devices with Anisotropic Optical Response: A Step toward Active Polarizer. *Nano Lett.* **2009**, *9*, 2144−2148.

(13) Michel, A. K. U.; Wuttig, M.; Taubner, T. Design Parameters for Phase-Change Materials for Nanostructure Resonance Tuning. *Adv. Opt. Mater.* **2017**, *5*, 1−8.

(14) Peng, J.; Jeong, H.; Lin, Q.; Cormier, S.; Liang, H.-L.; De Volder, M.; Vignolini, S.; Baumberg, J. Scalable Electrochromic Nano-Pixels Using Plasmonics. *Sci. Adv.* **2019**, *5*, eaaw2205.

(15) Flauraud, V.; Reyes, M.; Paniagua-Domínguez, R.; Kuznetsov, A. I.; Brugger, J. SiliconNanostructures for Bright Field Full Color Prints. *ACS Photonics* **2017**, *4*, 1913−1919.

(16) Roberts, A. S.; Pors, A.; Albrektsen, O.; Bozhevolnyi, S. I. Subwavelength Plasmonic Color Printing Protected for Ambient Use. *Nano Lett.* **2014**, *14*, 783−787.

DOI: 10.1021/acsphotonics.9b00716
ACS Photonics XXXX, XXX, XXX−XXX

(17) Zhu, X.; Vannahme, C.; Hojlund-Nielsen, E.; Mortensen, N. A.; Kristensen, A. Plasmonic Colour Laser Printing. *Nat. Nanotechnol.* **2016**, *11*, 325−329.
(18) Albrecht, G.; Ubl, M.; Kaiser, S.; Giessen, H.; Hentschel, M. Comprehensive Study of Plasmonic Materials in the Visible and Near-Infrared: Linear, Refractory, and Nonlinear Optical Properties. *ACS Photonics* **2018**, *5*, 1058−1067.
(19) Chan, G. H.; Zhao, J.; Hicks, E. M.; Schatz, G. C.; Van Duyne, R. P. Plasmonic Properties of Copper Nanoparticles Fabricated by Nanosphere Lithography. *Nano Lett.* **2007**, *7*, 1947−1952.
(20) Ambrose, J.; Barradas, R. G.; Shoesmith, D. W. Investigations of Copper in Aqueous Alkaline Solutions by Cyclic Voltammetry. *J. Electroanal. Chem. Interfacial Electrochem.* **1973**, *47*, 47−64.
(21) Teo, W. Z.; Ambrosi, A.; Pumera, M. Direct Electrochemistry of Copper Oxide Nanoparticles in Alkaline Media. *Electrochem. Commun.* **2013**, *28*, 51−53.
(22) Marchiano, S. L.; Elsner, C. I.; Arvia, A. J. The Anodic Formation and Cathodic Reduction of Cuprous Oxide Films on Copper in Sodium Hydroxide Solutions. *J. Appl. Electrochem.* **1980**, *10*, 365−377.
(23) Han, W.-K.; Choi, J.-W.; Hwang, G.-H.; Hong, S.-J.; Lee, J.-S.; Kang, S.-G. Fabrication of Cu Nano Particles by Direct Electrochemical Reduction from CuO Nano Particles. *Appl. Surf. Sci.* **2006**, *252*, 2832−2838.
(24) Yamukyan, M. H.; Manukyan, K. V.; Kharatyan, S. L. Copper Oxide Reduction by Hydrogen under the Self-Propagation Reaction Mode. *J. Alloys Compd.* **2009**, *473*, 546−549.
(25) Zentgraf, T.; Meyrath, T. P.; Seidel, A.; Kaiser, S.; Giessen, H.; Rockstuhl, C.; Lederer, F. Babinet's Principle for Optical Frequency Metamaterials and Nanoantennas. *Phys. Rev. B: Condens. Matter Mater. Phys.* **2007**, *76*, 33407.
(26) Hentschel, M.; Weiss, T.; Bagheri, S.; Giessen, H. Babinet to the Half: Coupling of Solid and Inverse Plasmonic Structures. *Nano Lett.* **2013**, *13*, 4428−4433.
(27) Knight, M. W.; King, N. S.; Liu, L.; Everitt, H. O.; Nordlander, P.; Halas, N. J. Aluminum for Plasmonics. *ACS Nano* **2014**, *8*, 834−840.
(28) Weiss, T.; Gippius, N. A.; Tikhodeev, S. G.; Granet, G.; Giessen, H. Derivation of Plasmonic Resonances in the Fourier Modal Method with Adaptive Spatial Resolution and Matched Coordinates. *J. Opt. Soc. Am. A* **2011**, *28*, 238−244.
(29) Keil, P.; Luetzenkirchen-Hecht, D.; Frahm, R. Investigation of Room Temperature Oxidation of Cu in Air by Yoneda-XAFS. *AIP Conference Proceedings* **2006**, *882*, 490.
(30) Software Spectra, Inc. Optical Data from Sopra SA; http://sspectra.com/sopra.html..
(31) NT&C. Bright-Field/Dark-Field Imaging/Spectroscopy Setup NanoMicroSpec, 2016; http://www.ntandc.de/spectroscopy.html.
(32) Dahlin, A. B.; Tegenfeldt, J. O.; Höök, F. Improving the Instrumental Resolution of Sensors Based on Localized Surface Plasmon Resonance. *Anal. Chem.* **2006**, *78*, 4416−4423.
(33) Wan, Y.; Zhang, Y.; Wang, X.; Wang, Q. Electrochemical Formation and Reduction of Copper Oxide Nanostructures in Alkaline Media. *Electrochem. Commun.* **2013**, *36*, 99−102.
(34) Yurkinskii, V. P.; Firsova, E. G.; Baturova, L. P. Corrosion Resistance of the Welded Joints of a Number of Structural Alloys in a NaOH Melt. *Russ. Metall.* **2015**, *2015*, 91−96.
(35) Bruggeman, D. A. G. Berechnung Verschiedener Physikalischer Konstanten von Heterogenen Substanzen. Dielektrizitaetskonstanten Und Leitfaehigkeit Der Mischkoerper Aus Isotropen Substanzen. *Ann. Phys.* **1935**, *416*, 636−664.
(36) Giebels, I. A. M. E.; Isidorsson, J.; Griessen, R. Highly Absorbing Black Mg and Rare-Earth-Mg Switchable Mirrors. *Phys. Rev. B: Condens. Matter Mater. Phys.* **2004**, *69*, 205111.
(37) Jiang, N.; Zhuo, X.; Wang, J. Active Plasmonics: Principles, Structures, and Application. *Chem. Rev.* **2018**, *118*, 3054−3099.
(38) Tittl, A.; Mai, P.; Taubert, R.; Dregely, D.; Liu, N.; Giessen, H. Palladium-Based Plasmonic Perfect Absorber in the Visible Wavelength Range and Its Application to Hydrogen Sensing. *Nano Lett.* **2011**, *11*, 4366−4369.
(39) Liu, N.; Mesch, M.; Weiss, T.; Hentschel, M.; Giessen, H. Infrared Perfect Absorber and Its Application as Plasmonic Sensor. *Nano Lett.* **2010**, *10*, 2342−2348.
(40) Luk'yanchuk, B.; Zheludev, N. I.; Maier, S. A.; Halas, N. J.; Nordlander, P.; Giessen, H.; Chong, C. T. The Fano Resonance in Plasmonic Nanostructures and Metamaterials. *Nat. Mater.* **2010**, *9*, 707−715.

DOI: 10.1021/acsphotonics.9b00716
ACS Photonics XXXX, XXX, XXX−XXX